2017

Ce0.8Sm0.2O1.9 decorated with electron-blocking acceptor-doped BaCeO3 as electrolyte for low-temperature solid oxide fuel cells

Zheng Gong
University of Science and Technology of China

Wenping Sun
University of Wollongong, wenping@uow.edu.au

Jiafeng Cao
University of Science and Technology of China

Duo Shan
University of Science and Technology of China

Yusen Wu
University of Science and Technology of China

See next page for additional authors

Publication Details

Gong, Z., Sun, W., Cao, J., Shan, D., Wu, Y. & Liu, W. (2017). Ce0.8Sm0.2O1.9 decorated with electron-blocking acceptor-doped BaCeO3 as electrolyte for low-temperature solid oxide fuel cells. Electrochimica Acta, 228 226-232.

Ce0.8Sm0.2O1.9 decorated with electron-blocking acceptor-doped BaCeO3 as electrolyte for low-temperature solid oxide fuel cells

Abstract

A series of composites with nominal compositions of BaCe0.8Sm0.2O3-δ (BCS)-Ce0.8Sm0.2 O1.9 (SDC) (20:80, 35:65, 50:50, 65:35 wt.%) are synthesized by a modified citric acid-nitrate sol-gel combustion method and evaluated as the electrolytes for low-temperature solid oxide fuel cells (SOFCs). The TEM results show that doped BaCeO3 decorated SDC particles are formed after calcining at 1000 °C for 3 h. X-ray diffraction results reveal that the composites are only composed of BaCeO3-based and SDC phases without any other impurity phases. Besides, BaCeO3-based phase is uniformly distributed in the sintered electrolytes according to EDS element mapping. The open cell voltages (OCVs) of the single cells increase gradually with increasing the proportion of BaCeO3-based phase, and are higher than those for bare SDC-based cells. Besides, the power performances of the cells are superior to SDC-based cells when BaCeO3-based phase is lower than 35 wt.%. Electrochemical impedance spectroscopy analysis indicates that, in addition to blocking electronic current leakage, BaCeO3-based phase would induce higher ohmic and polarization resistance, which is detrimental to power performance. Further specific effort should be focused on synthesizing uniform SDC@BCS core-shell electrolyte powders and minimizing the proportion of BCS phase towards high-performance SOFCs with high OCVs.

Disciplines

Engineering | Physical Sciences and Mathematics

Publication Details

Gong, Z., Sun, W., Cao, J., Shan, D., Wu, Y. & Liu, W. (2017). Ce0.8Sm0.2O1.9 decorated with electron-blocking acceptor-doped BaCeO3 as electrolyte for low-temperature solid oxide fuel cells. Electrochimica Acta, 228 226-232.

Authors

Zheng Gong, Wenping Sun, Jiafeng Cao, Duo Shan, Yusen Wu, and Wei Liu

$Ce_{0.8}Sm_{0.2}O_{1.9}$ decorated with electron-blocking acceptor-doped $BaCeO_3$ as electrolyte for low-temperature solid oxide fuel cells

Zheng Gong[a], Wenping Sun[b,*], Jiafeng Cao[a], Duo Shan[a], Yusen Wu[a], Wei Liu[a,c,*]

[a]CAS Key Laboratory of Materials for Energy Conversion & Collaborative Innovation Center of Suzhou Nano Science and Technology, University of Science and Technology of China, Hefei 230026, PR China

[b]Institute for Superconducting and Electronic Materials, Australian Institute of Innovative Materials, University of Wollongong, Wollongong, NSW 2522, Australia

[c]Key Laboratory of Materials Physics, Institute of Solid State Physics, Chinese Academy of Sciences, Hefei 230031, PR China

[*] Corresponding author.
E-mail address: wenping@uow.edu.au (W. Sun), wliu@ustc.edu.cn (W. Liu).

Abstract

A series of composites with nominal compositions of $BaCe_{0.8}Sm_{0.2}O_{3-\delta}$ (BCS)-$Ce_{0.8}Sm_{0.2}O_{1.9}$ (SDC) (20:80, 35:65, 50:50, 65:35 wt.%) are synthesized by a modified citric acid-nitrate sol-gel combustion method and evaluated as the electrolytes for low-temperature solid oxide fuel cells (SOFCs). The TEM results show that doped $BaCeO_3$ decorated SDC particles are formed after calcining at 1000 °C for 3 h. X-ray diffraction results reveal that the composites are only composed of $BaCeO_3$-based and SDC phases without any other impurity phases. Besides, $BaCeO_3$-based phase is uniformly distributed in the sintered electrolytes according to EDS element mapping. The open cell voltages (OCVs) of the single cells increase gradually with increasing the proportion of $BaCeO_3$-based phase, and are higher than those for bare SDC-based cells. Besides, the power performances of the cells are superior to SDC-based cells when $BaCeO_3$-based phase is lower than 35 wt.%. Electrochemical impedance spectroscopy analysis indicates that, in addition to blocking electronic current leakage, $BaCeO_3$-based phase would induce higher ohmic and polarization resistance, which is detrimental to power performance. Further specific effort should be focused on synthesizing uniform SDC@BCS core-shell electrolyte powders and minimizing the proportion of BCS phase towards high-performance SOFCs with high OCVs.

Keywords: Composite electrolyte; Solid oxide fuel cells; In-situ reaction; Open circuit voltage; Mixed ion conductor;

1. Introduction

Solid oxide fuel cell (SOFC) as an efficient and clean electrochemical energy conversion device has received increasing attention over the past several decades [1-3]. Although great development of SOFC has been made, the high operating temperature is still a major problem, which results in high fabrication cost and limits the selection of materials, consequently hindering its commercial application [4, 5]. Recently, many efforts have been devoted to reducing the operating temperature to intermediate/lower temperatures. Decreasing electrolyte thickness and employing electrolyte materials with higher ionic conductivity are two main approaches [6]. Among currently developed oxide ionic conductors, samaria-doped ceria (SDC) is considered to be a promising electrolyte material due to its high ionic conductivity at reduced temperature and excellent chemical compatibility with most cathode materials, which is extensively investigated for intermediate/low temperature SOFC [7, 8]. However, the open circuit voltages (OCVs) of SDC-based SOFC are obviously lower than theoretical Nernst voltages, which are induced by the reduction of Ce^{4+} to Ce^{3+} in SDC electrolyte under working condition [9, 10]. Besides, the partial reduction of Ce^{4+} would also result in mechanical failure of the electrolyte owning to the mismatching of ionic radius of Ce^{4+} and Ce^{3+}.

In order to protect the SDC electrolyte from reduction at the anode side, different approaches have been developed. The frequently-used strategy is to incorporate a dense blocking layer between the anode and SDC electrolyte [11, 12]. For example, when a thin layer of yttria-stabilized zirconia (YSZ), a typical oxygen ion conductor

electrolyte, was used to block the reduction of SDC, the OCV was significantly increased (~1.0 V at 700 °C) and approached to theoretical Nernst voltages [13]. Except for typical oxide ionic conductors, doped $BaCeO_3$ including $BaZr_{0.1}Ce_{0.7}Y_{0.2}O_{3-\delta}$ (BZCY) [14] and $BaCe_{0.8}Y_{0.2}O_{3-\delta}$ (BCY) [15], mixed proton-oxide ion conductors, have been demonstrated to block electronic conduction through doped ceria oxides (DCO) electrolyte membrane. However, the fabrication process of the bi-layered electrolytes is complicated and the long-term stability might be a problem on account of the difference of the thermal expansion coefficient (TEC) of the electrolytes, and the electrochemical performance is not competitive as compared with those typical doped-ceria-based cells due to the low oxygen-ionic conductivity of YSZ and doped $BaCeO_3$. In addition, replacing traditional NiO-SDC anode with Ba-containing composites, such as NiO-BZCY [7], NiO-$BaZr_{0.45}Ce_{0.45}Gd_{0.1}O_{3-\delta}$ (BZCG) [16], and NiO-BZCG-GDC [17], also turn out to be an practical strategy since electron-blocking layer can be in-situ formed during sintering process utilizing Ba ion diffusion from anode side to reaction with DCO electrolyte membrane in the interface.

Recently, a composite electrolyte materials consisting of DCO and doped $BaCeO_3$ were extensively investigated and deemed to be a more simple and effective means to eliminate the internal short-circuit behavior, e.g. $Ce_{0.8}Nd_{0.2}O_{2-\delta}$-$BaCe_{0.8}Nd_{0.2}O_{3-\delta}$ [18], SDC-$BaCe_{0.8}Sm_{0.2}O_{3-\delta}$ (BCS) [19], and the coking resistant can be significantly enhanced when the composite is employed as anode material [20]. As reported by Sun et.al [19], the BCS grains in the composite

can protect the SDC from reduction, and single cells based on the composite electrolyte exhibited high OCV values (0.971 V at 650 °C) and good performance stability when H_2 was used as the fuel. However, the electrochemical performance was not very promising for practical application. For instance, the peak power density of a cell based on the composite electrolyte was only 345 $mWcm^{-2}$ at 650 °C. Besides, there are almost no researches focused on the reasons for such poor electrochemical performance.

It was demonstrated that the $BaCe_{1-x}Sm_xO_{3-\delta}$ layer can be formed by a solid-state reaction between BaO and SDC electrolyte layer at elevated temperatures [21]. Herein we report an innovative nanocomposite electrolyte SDC decorated with BCS phase, which differs from the reported BCS-SDC composite electrolyte prepared via a one-pot process [19, 22, 23]. The composite electrolyte powders were synthesized by combining a modified citric acid-nitrate sol-gel combustion method and in-situ solid-state reaction for the first time. The feasibility of in-situ formed composite as electrolyte for SOFC were evaluated, and the effect of the nominal BCS content on the electrochemical performance of single cells were also investigated. The encouraging results provide a new strategy to design composite electrolytes for SOFCs.

2. Experimental

2.1. Powders synthesis and cell fabrication

Nominal compositions of $BaCe_{0.8}Sm_{0.2}O_{3-\delta}$ (BCS)-$Ce_{0.8}Sm_{0.2}O_{1.9}$ (SDC) with a weight ratio of 20:80, 35:65; 50:50 and 65:35 were all synthesized by combining a

modified citric acid-nitrate sol-gel combustion method [24] and in-situ solid-state reaction. The synthesis schematic diagram is shown in Fig.1. Firstly, $Ba(CH_3COO)_2$ was dissolved in dilute nitric acid under stirring at about 80 °C, then a certain amount of citric acid was added into the solution and aqueous ammonia was used to control the pH of the solution to about 8. Subsequently, SDC powders calcined at 600 °C for 3 h prepared by a gel combustion process [25] was added into the solution in proportion.

The solution was then moved to an evaporating dish on a hot pate until it combusted automatically. Finally, the as-prepared powder was calcined at 1000 °C for 3 h to form nanocomposite electrolyte. The anode-supported half cells with the structure of NiO-SDC|BCS-SDC were fabricated by a dry-pressing method [26] and then co-fired at 1400 °C for 5 h. 20 wt.% starch used as pore former was added into the anode substrate. Typical cathode slurry $Sm_{0.5}Sr_{0.5}CoO_{3-\delta}$ (SSC)-SDC with a weight ratio of 6:4 was brushed on the half cells, and then fired at 950 °C for 2 h to form a porous layer with an active area of 0.237 cm^2.

2.2. Characterization of materials and electrochemical testing of single cells

The phase structures of the synthetic powders were characterized by X-ray diffractometer with Cu Kα radiation. Transmission electron microscopy (TEM, JEM-2010) and scanning electron microscopy (SEM, JEOL JSM-6700F) equipped with an energy-dispersive X-ray spectroscopy (EDS) system were employed to observe the morphology of the powders and cell microstructures. All fabricated cells were measured in a home-made testing device from 650 to 450 °C with ~3% H_2O

humidified hydrogen (40 mL min^{-1}) as the fuel and static air as the oxidant. The current-voltage (I-V) curves of the cells were measured by using a DC Electronic Load. A.C impedance spectra were collected by a CHI604E impedance analyzer under open circuit condition in the frequency range from 100 kHz to 0.1 Hz, and a 5 mV amplitude signal was applied.

3. Results and discussion

To gain insight into the reaction process during the formation of BCS-SDC composite, XRD characterization of the synthesized powders before and after calcination was performed. Except for the synthesized BCS-SDC (50:50 wt.%) composite powders, the XRD patterns of the prepared SDC powders calcined at 600 °C for 3 h, $BaCO_3$ (PDF 05-0378) and $BaCeO_3$ (PDF 35-1318) are also presented in Fig.2a for clear comparison. One can see that the diffraction pattern of the as-prepared powders matches well with that of SDC and $BaCO_3$. When the powders were calcined at 1000 °C for 3 h, the characteristic peaks of $BaCO_3$ phase disappeared completely along with the formation of doped $BaCeO_3$ phase. Thus, we can conclude that the as-prepared powders consist of SDC and $BaCO_3$ phases, while the BCS-SDC composite is composed of SDC and $BaCe_{1-x}Sm_xO_{3-\delta}$ phase obtained via the in-situ solid state reaction, and the possible reactions are described as follows:

$$BaCO_3 \rightarrow BaO + CO_2\uparrow \quad [1]$$

$$BaO + Ce_{0.8}Sm_{0.2}O_{1.9} \rightarrow BaCe_{1-x}Sm_xO_{3-\delta} \quad [2]$$

The XRD patterns of the composites with different nominal weight ratio of BCS calcined at 1000 °C for 3 h are shown in Fig.2b, and only diffraction peaks

corresponding to SDC and BCS can be found in all the patterns. Moreover, with increasing Ba content, the (110) peak intensity at about 28.70º, which is identified as the main peak of the $BaCeO_3$ phase increases accordingly, whereas the intensity of the (111) peak of the SDC phase at 28.40° decreases gradually (Fig.2c), demonstrating that more SDC is consumed and involved in the in-situ solid state reaction accompanying with the formation of $BaCe_{1-x}Sm_xO_{3-\delta}$ phase according to the equation 2.

Shown in Fig.3a is a typical SEM image of the BCS-SDC (50:50 wt.%) composite after calcined at 1000 °C for 3 h. The uniform particles are smaller than 100 nm and agglomerate loosely together. This makes it easy to be crushed to fine powders with good sintering activity. Fig.3b HRTEM image of the composite powders. As can be seen from the HRTEM image, the SDC nanoparticles are partly coated by a thin layer of $BaCe_{1-x}Sm_xO_{3-\delta}$ instead of isolated nanoparticles. The lattice spacings of 0.32 and 0.31 nm corresponds to the (111) and (110) crystal plane of SDC and $BaCe_{1-x}Sm_xO_{3-\delta}$, respectively. The HRTEM results indicated that core-shell structure SDC@doped $BaCeO_3$ nanoparticles are formed via the in-situ solid state reaction. It has to be mentioned that isolated $BaCe_{1-x}Sm_xO_{3-\delta}$ particles should also account for considerable proportion. The $BaCe_{1-x}Sm_xO_{3-\delta}$ phase would effectively protect SDC from reduction, and eventually prevent electronic current leakage across the electrolyte, resulting in improved OCVs for single cells. Fig.4 shows the EDS mapping of the cross-section of the sintered dense BCS-SDC (50:50 wt.%) electrolyte. Clearly, Ba, Ce, and Sm elements distribute uniformly across the electrolyte

membrane. The result suggests that the SDC and BCS phases have at least a homogeneous distribution in the electrolyte at the submicron level.

In order to evaluate the BCS-SDC composite electrolytes, anode-supported single cells with Ni-SDC anode and SSC-SDC cathode were tested from 650 to 450 °C using wet H_2 as the fuel and static air as the oxidant. Fig.5 shows SEM images of the cross-section of the tested single cells with different electrolytes and electrolyte surface. One can see that all the electrolyte membranes of the single cells are fully dense, crack-free and closely bonded with the anode support and cathode layer. Moreover, the cells have almost identically thick electrolyte (~30 μm) and SSC-SDC cathode (~18 μm) except that the electrolyte thickness of the typical SDC-based cell is about 25 μm. The OCVs of the single cells with different electrolytes are presented in Fig.6. As expected, the OCV values are significantly higher than those for the SDC-based cell and increase with increasing the BCS amount in the composites. The OCV increment suggests that the electronic current across SDC particles is partly blocked by BCS particles in the composite electrolytes, which is consistent with the previously reported results [19, 27].

The I-V and I-P curves of the single cells with different composite electrolytes as well as SDC electrolyte are plotted in Fig.7. When BCS-SDC (20:80 wt.%) composite was used as the electrolyte, the peak power densities (PPDs) of the cell are 786, 613, 422, 252, and 127 $mWcm^{-2}$ at 650,600, 550, 500 and 450 °C, respectively, as shown in Fig.7a, which outputs much higher PPDs than the previously reported similar SOFCs with composite electrolytes [19, 23, 27-31], as shown in Table 1. With

increasing the mass fraction of BCS to 35%, the PPD decreases to 695, 515, 326, 171 and 76 $mWcm^{-2}$ at 650,600, 550, 500 and 450 °C, respectively, as shown in Fig.7b. It should be noted that the PPDs are still higher than that of the typical cell based on SDC electrolyte (Fig.7e), though the SDC cell has a thinner electrolyte (Fig. 6e). For clear comparison, the I-V and I-P curves of the cells with different composite electrolytes tested at 650 °C are plotted in Fig.7f. The PPDs of single cells with BCS-SDC (50:50 wt.%) , BCS-SDC (65:35 wt.%) and SDC as electrolyte are 415, 277 and 636 $mWcm^{-2}$ at 650 °C, respectively. With further increasing the BCS proportion in the composite electrolytes to be greater than 35 wt.%, one can see that the PPDs decreases significantly and are inferior to the typical SDC-based cell. Although the power performances of the cells decrease with the increase of BCS mass fraction, introducing small amount of BCS into SDC electrolyte is beneficial to enhance electrochemical performances of a single cell including higher power densities and improved OCV values compared with SDC-based SOFC. The similar phenomenon was also found in pervious reported composite electrolytes based on $BaO\text{-}CeO_2\text{-}GdO_{1.5}$ ternary system [27]. In view of the above experimental results, the BCS-SDC (20:80 wt.%) and BCS-SDC (35:65 wt.%) may be alternative composites for use as electrolytes for low-temperature SOFCs, and the in-situ solid state reaction may be a potential strategy to design composite electrolyte.

To further understand how the composition variation of the electrolytes causes the performance difference, electrochemical impedance spectra (EIS) of the cells at 650 °C were measured under open circuit conditions and shown in Fig.8a and b. The

high-frequency intercept represents the ohimc resistance (R_o), which is mainly contributed by the electrolyte resistance, while the difference between high-frequency and low-frerquency intercepts corresponds to the polarization resistance (R_p). The R_o of the cells with BCS-SDC (20:80 wt.%) , BCS-SDC (35:65 wt.%) , BCS-SDC (50:50 wt.%) , BCS-SDC (65:35 wt.%) and SDC as electrolyte is calculated to be 0.172, 0.186, 0.246, 0.483, and 0.178 Ωcm^2, while R_p is 0.078, 0.081, 0.183, 0.185, and 0.052 Ωcm^2 at 650 °C, respectively. It can be found that R_o and R_p increase remarkedly with increasing BCS in the composite electrolyte. With repect to R_p, the high-frequency resistance that corresponds to charge transfer [32] exhibit more significant dependence on BCS proportion. Considering all the cells are fabricated and tested under same conditions, the increment of R_o and R_p can be ascribed to the gradually decreased ionic conductivity of the composite electrolyte, and this is the main reason that results in the decrease of the power performances of the cells as discussed before. The partially elimination of the internal short circuit current through the electrolyte membrane also leaded to the increase of R_p to a certain extent [7]. As widely reportedly, the improvement of OCV is beneficial to deliver higher PPDs [1, 33], according to the following formulas:

$$P = IV = I(V_{ocv} \quad IR_t) \quad (3)$$

$$P_{max} = \frac{V_{ocv}^2}{4R_t} \quad (4)$$

Where V is output cell potential, I is current, V_{ocv} is the open circuit voltage, the R_t is the total resistance of the cell, and the P_{max} is the maximum power density. Under given conditions, R_t is a constant, one can see that higher OCV will lead to higher

P_{max} from Eq. (4). Therefore, there is a balance between OCV and cell resistance to eventually achieve promising PPDs for the cells with such BCS-SDC composite electrolytes.

In order to verify the durability of BCS-SDC electrolyte, the short-term stability of the single cells were tested and shown in Fig.9. The power density was about 520 $mWcm^{-2}$ under the cell voltage of 0.6 V and the OCV value was 0.86 V at 600 °C. One can see that no degradation was observed during the period of testing, indicating that BCS-SDC electrolyte is chemical stability in operating condition, which is consistent with the reported work for the similar composite compound [34].

Conclusions

In summary, doped $BaCeO_3$ decorated SDC particles were successfully synthesized via in-situ solid reaction for the first time. The XRD and TEM results demonstrated the BCS phase was in-situ formed on the surface of SDC particles and without any other impurity phase exist. The BCS particles in the composite can effectively block the electronic current across SDC under SOFC operation conditions, and, consequently, the OCVs of the single cells were improved and higher than that of SDC-based cells. It has to be noted that BCS phase would increase the ohmic and polarization resistance of the cell. The results demonstrate that compared with SDC, BCS-SDC composite with a certain amount of BCS is a promising alternative as an electrolyte for low-temperature SOFCs with high power densities and improved OCVs.

Acknowledgments

This work was supported by the National Science Foundation of China (Grant Nos: 21676261 and U1632131) and the Fundamental Research Funds for the Central Universities (Grant No.WK6030000016).

References

[1] E.D. Wachsman, K.T. Lee, Science 334 (2011) 935-939.

[2] B.C.H. Steele, A. Heinzel, Nature 414 (2001) 345-352.

[3] D.A. Medvedev, J.G. Lyagaeva, E.V. Gorbova, A.K. Demin, P. Tsiakaras, Prog. Mater. Sci. 75 (2016) 38-79.

[4] D.J. Brett, A. Atkinson, N.P. Brandon, S.J. Skinner, Chem. Soc. Rev. 37 (2008) 1568-1578.

[5] Y. Chen, W. Zhou, D. Ding, M. Liu, F. Ciucci, M. Tade, Z. Shao, Adv. Energy Mater. 5 (2015) 1500537-1500570.

[6] L. Malavasi, C.A. Fisher, M.S. Islam, Chem. Soc. Rev. 39 (2010) 4370-4387.

[7] W.P. Sun, W. Liu, J. Power Sources 217 (2012) 114-119.

[8] Z.P. Shao, S.M. Haile, Nature 431 (2004) 170-173.

[9] X. Zhang, M. Robertson, C. Deces-Petit, W. Qu, O. Kesler, R. Maric, D. Ghosh, J. Power Sources 164 (2007) 668-677.

[10] T. Matsui, T. Kosaka, M. Inaba, A. Mineshige, Z. Ogumi, Solid State Ionics 176 (2005) 663-668.

[11] J. Qian, Z. Tao, J. Xiao, G. Jiang, W. Liu, Int. J. Hydrogen Energ. 38 (2013) 2407-2412.

[12] H.T. Lim, A.V. Virkar, J. Power Sources 192 (2009) 267-278.

[13] J. Qian, Z.W. Zhu, J.J. Dang, G.S. Jiang, W. Liu, Electrochim. Acta 92 (2013) 243-247.

[14] W.P. Sun, Z. Shi, Z.T. Wang, W. Liu, J. Membrane Sci. 476 (2014) 394-398.

[15] H. Sumi, E. Suda, M. Mori, Int. J. Hydrogen Energ. (2016), http://dx.doi.org/10.1016/j.ijhydene.2016.09.176.

[16] J.F. Cao, Z. Gong, J. Hou, J.F. Cao, W. Liu, Ceram. Int. 41 (2015) 6824-6830.

[17] J. Cao, Z. Gong, C. Fan, Y. Ji, W. Liu, J. Alloy Compd. 693 (2017) 1068-1075.

[18] D. Medvedev, E. Pikalova, A. Demin, A. Podias, I. Korzun, B. Antonov, P. Tsiakaras, J. Power Sources 267 (2014) 269-279.

[19] W. Sun, Y. Jiang, Y. Wang, S. Fang, Z. Zhu, W. Liu, J. Power Sources 196 (2011) 62-68.

[20] Z. Tao, G. Hou, N. Xu, Q. Zhang, H. Ding, Electrochim. Acta 150 (2014) 55-61.

[21] D. Hirabayashi, A. Tomita, T. Hibino, M. Nagao, M. Sano, Electrochem. Solid-State Lett. 7 (2004) A318-A320.

[22] D. Medvedev, V. Maragou, E. Pikalova, A. Demin, P. Tsiakaras, J. Power Sources 221 (2013) 217-227.

[23] D. Tian, W. Liu, Y. Chen, Q. Gu, B. Lin, Ionics 21 (2014) 823-828.

[24] W. Sun, M. Liu, W. Liu, Adv. Energy Mater. 3 (2013) 1041-1050.

[25] W. Sun, Z. Shi, W. Liu, J. Electrochem. Soc. 160 (2013) F585-F590.

[26] Z. Gong, W.P. Sun, D. Shan, Y.S. Wu, W. Liu, ACS Appl. Mater. Inter. 8 (2016) 10835-10840.

[27] A. Venkatasubramanian, P. Gopalan, T.R.S. Prasanna, Int. J. Hydrogen Energ. 35

(2010) 4597-4605.

[28] F. Liu, J. Dang, J. Hou, J. Qian, Z. Zhu, Z. Wang, W. Liu, J. Alloy Compd. 639 (2015) 252-258.

[29] B. Zhu, X. Liu, T. Schober, Electrochem. Commun. 6 (2004) 378-383.

[30] D. Lin, Q. Wang, K. Peng, L.L. Shaw, J. Power Sources 205 (2012) 100-107.

[31] B. Li, S. Liu, X. Liu, S. Qi, J. Yu, H. Wang, W. Su, Int. J. Hydrogen Energ. 39 (2014) 14376-14380.

[32] K. Zhao, Q. Xu, D.-P. Huang, M. Chen, B.-H. Kim, J. Solid State Electr. 16 (2012) 2797-2804.

[33] W. Sun, Y. Wang, S. Fang, Z. Zhu, L. Yan, W. Liu, Electrochim. Acta 56 (2011) 1447-1454.

[34] D. Hirabayashi, A. Tomita, S. Teranishi, T. Hibino, M. Sano, Solid State Ionics 176 (2005) 881-887.

Captions

Figure 1 Schematic diagram of synthesis process for the nanocomposite electrolyte BCS-SDC

Figure 2 XRD patterns of (a) the as-prepared BCS-SDC, SDC and BCS-SDC powder as well as the $BaCO_3$ and $BaCeO_3$, (b) the BCS-SDC composites with different composition, and (c) magnified XRD patterns for $22^{o} \leq 2\theta \leq 38^{o}$.

Figure 3 (a) SEM, (b) HRTEM images of the BCS-SDC (50:50 wt.%) calcined at 1000 °C for 3 h

Figure 4 SEM image of the cross-section of BCS-SDC electrolyte membrane, and

corresponding EDS element mapping data of Ba, Ce, and Sm.

Figure 5 Cross-sectional SEM images of the cells with (a) BCS-SDC (20:80 wt.%), (b) BCS-SDC (35:65 wt.%), (c) BCS-SDC (50:50 wt.%), (d) BCS-SDC (65:35 wt.%), (e) SDC as electrolyte, and (f) the surface of BCS-SDC (50:50 wt.%) electrolyte membrane.

Figure 6 The OCVs of the single cells with SDC and series of BCS-SDC composites as electrolyte.

Figure 7 I-V and I-P curves of the cells with (a) BCS-SDC (20:80 wt.%), (b) BCS-SDC (35:65 wt.%), (c) BCS-SDC (50:50 wt.%), (d) BCS-SDC (65:35 wt.%), and (e) SDC as electrolyte, as well as (f) I-V and I-P curves of the cells with different electrolyte tested at 650 °C

Figure 8 (a) EIS of the cells with different electrolyte are measured under open circuit conditions at 650 °C, and (b) comparison of the EIS spectra after subtracted R_o

Figure 9 (a) Short-term stability of the single cell with BCS-SDC (20:80 wt.%) as the electrolyte tested under cell voltage of 0.6 V, and (b) OCV tested under open condition at 600 °C

Table1 Summary of the maximum power density (MPD), open circuit voltage (OCV), ohmic (R_o) and polarization resistance (R_p) of the composite electrolyte based SOFCs reported in literature

Fig.1

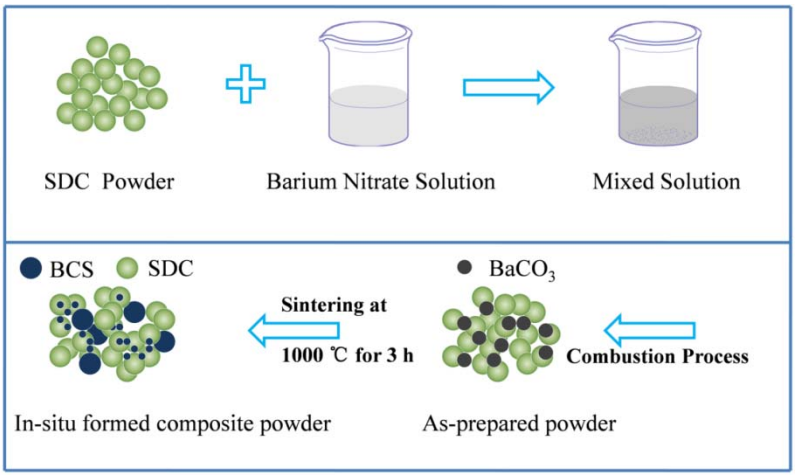
SDC Powder
Barium Nitrate Solution
Mixed Solution
BCS
SDC
Sintering at
1000 ℃ for 3 h
$BaCO_3$
Combustion Process
In-situ formed composite powder
As-prepared powder

Fig.2

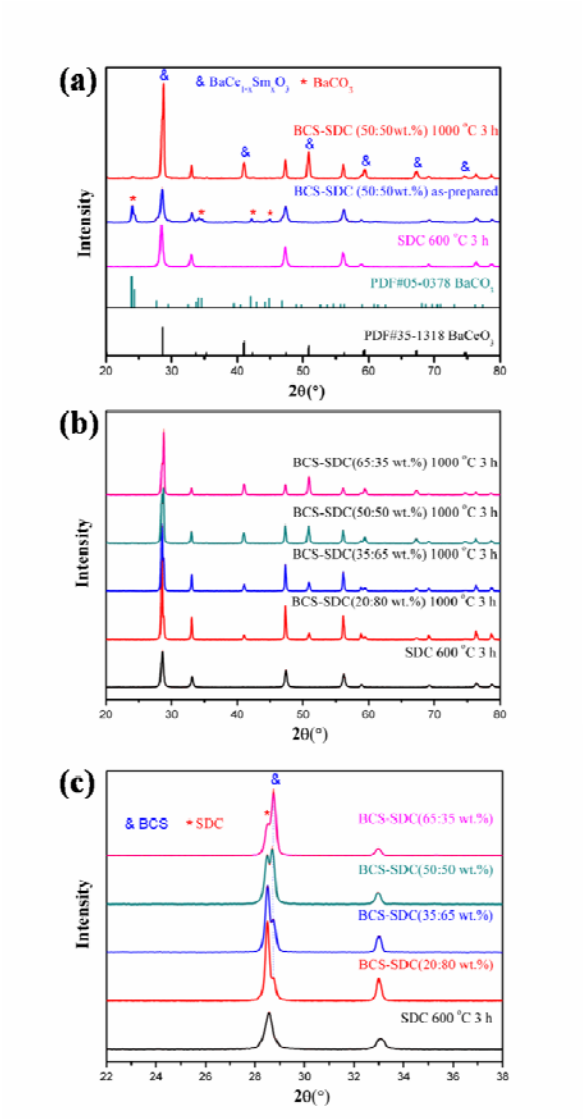
(a)
& $BaCe_{1-x}Sm_xO_3$ * $BaCO_3$
BCS-SDC (50:50wt.%) 1000 °C 3 h
BCS-SDC (50:50wt.%) as-prepared
SDC 600 °C 3 h
PDF#05-0378 $BaCO_3$
PDF#35-1318 $BaCeO_3$
Intensity
2θ(°)
(b)
BCS-SDC(65:35 wt.%) 1000 °C 3 h
BCS-SDC(50:50 wt.%) 1000 °C 3 h
BCS-SDC(35:65 wt.%) 1000 °C 3 h
BCS-SDC(20:80 wt.%) 1000 °C 3 h
SDC 600 °C 3 h
Intensity
2θ(°)
(c)
& BCS * SDC
BCS-SDC(65:35 wt.%)
BCS-SDC(50:50 wt.%)
BCS-SDC(35:65 wt.%)
BCS-SDC(20:80 wt.%)
SDC 600 °C 3 h
Intensity
2θ(°)

Fig.3

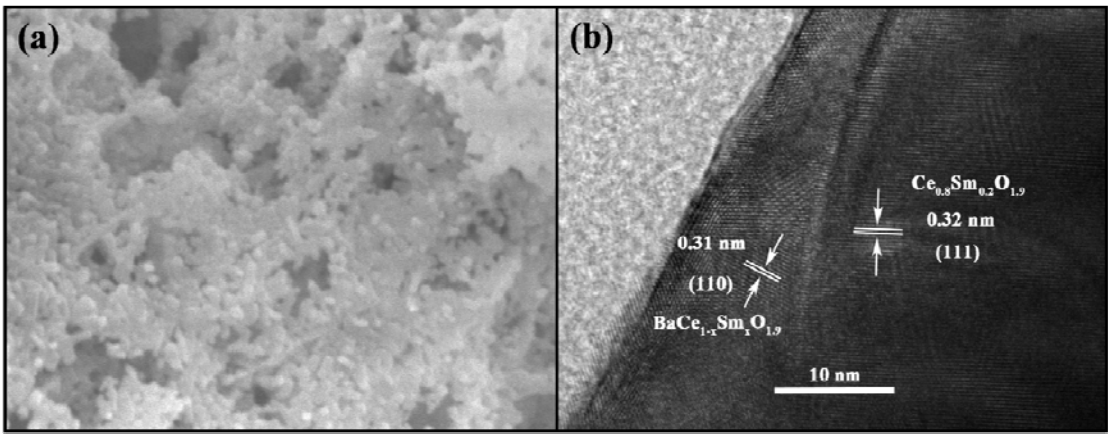
(a)
(b)
$Ce_{0.8}Sm_{0.2}O_{1.9}$
0.32 nm
(111)
0.31 nm
(110)
$BaCe_{1-x}Sm_xO_{1.9}$
10 nm

Fig.4

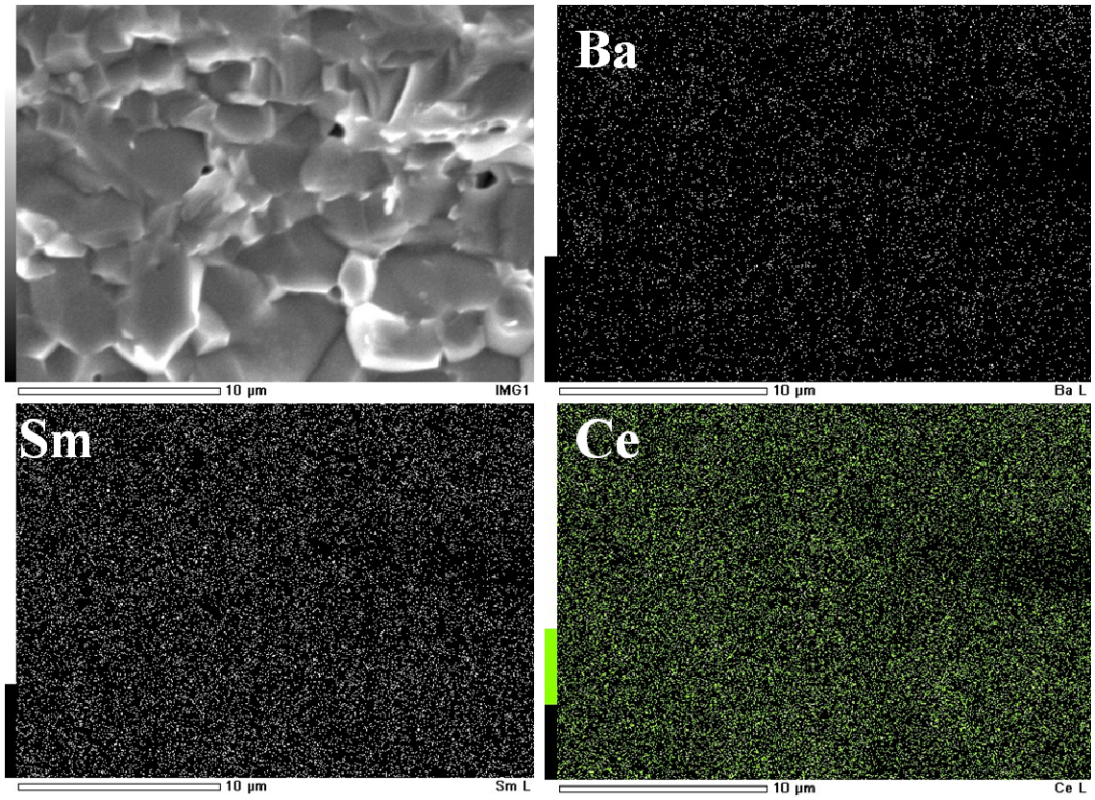
10 μm
IMG1
Ba
10 μm
Ba L
Sm
10 μm
Sm L
Ce
10 μm
Ce L

Fig.5

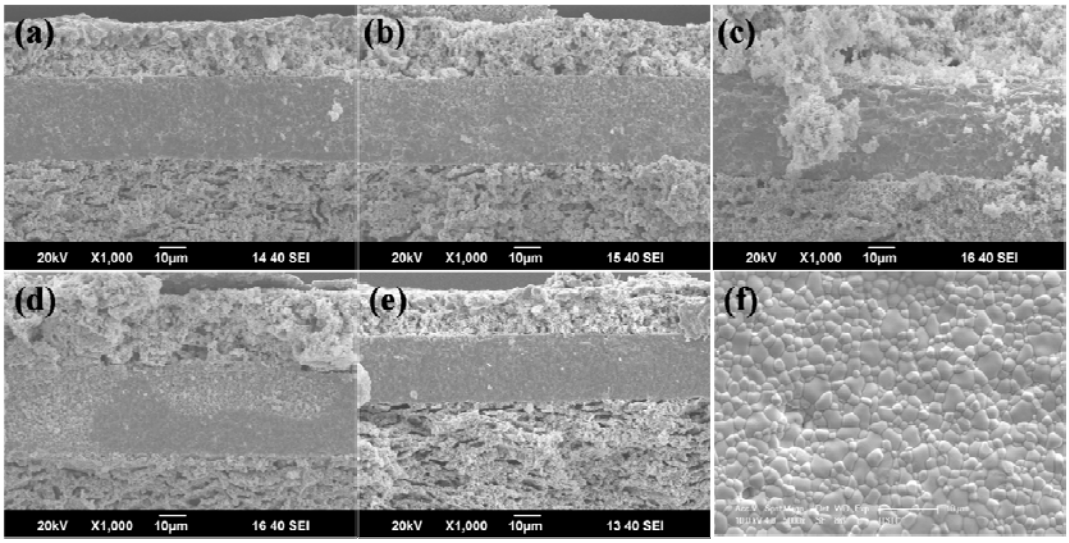
(a)
(b)
(c)
(d)
(e)
(f)
20kV X1,000 10μm 14 40 SEI
20kV X1,000 10μm 15 40 SEI
20kV X1,000 10μm 16 40 SEI
20kV X1,000 10μm 16 40 SEI
20kV X1,000 10μm 13 40 SEI

Fig.6

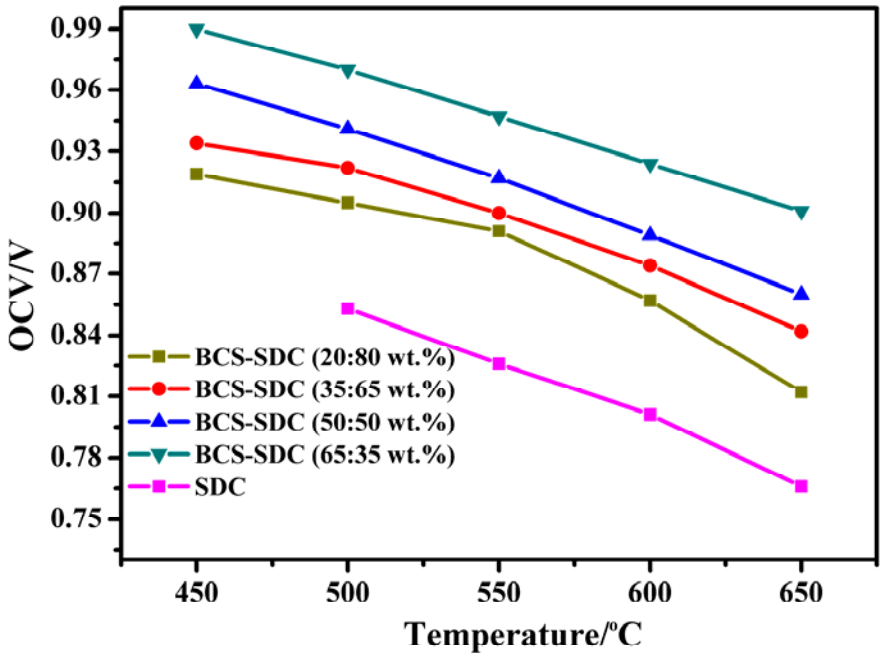
OCV/V
0.99
0.96
0.93
0.90
0.87
0.84
0.81
0.78
0.75
450
500
550
600
650
Temperature/°C
BCS-SDC (20:80 wt.%)
BCS-SDC (35:65 wt.%)
BCS-SDC (50:50 wt.%)
BCS-SDC (65:35 wt.%)
SDC

Fig.7

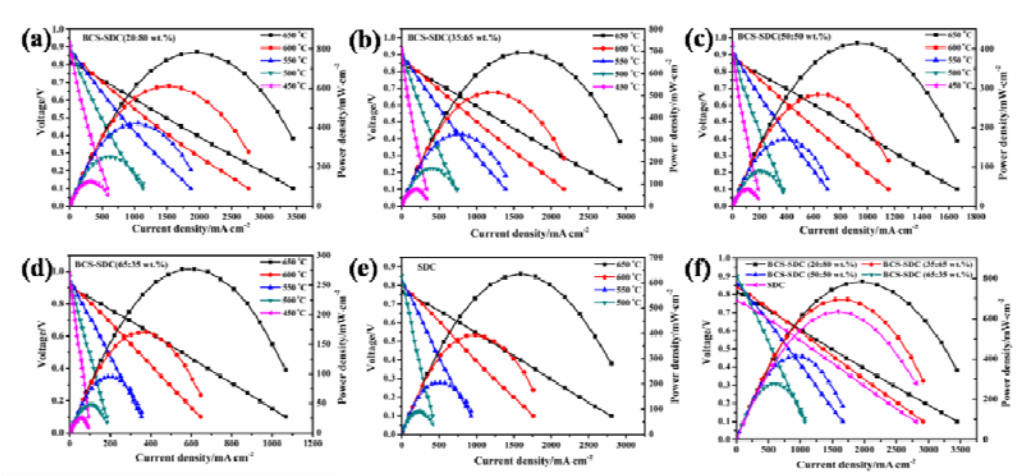
(a)
(b)
(c)
(d)
(e)
(f)
Voltage/V
Power density/mW cm-2
Current density/mA cm-2
SDC

Fig.8

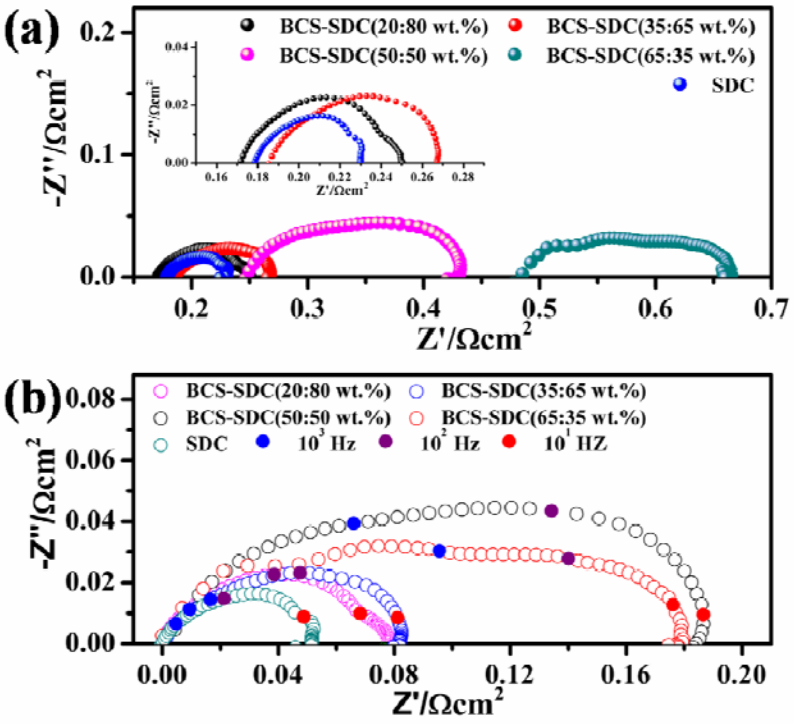
(a)
BCS-SDC(20:80 wt.%)
BCS-SDC(35:65 wt.%)
BCS-SDC(50:50 wt.%)
BCS-SDC(65:35 wt.%)
SDC
-Z''/Ωcm2
Z'/Ωcm2
(b)
10^3 Hz
10^2 Hz
10^1 HZ

Fig.9

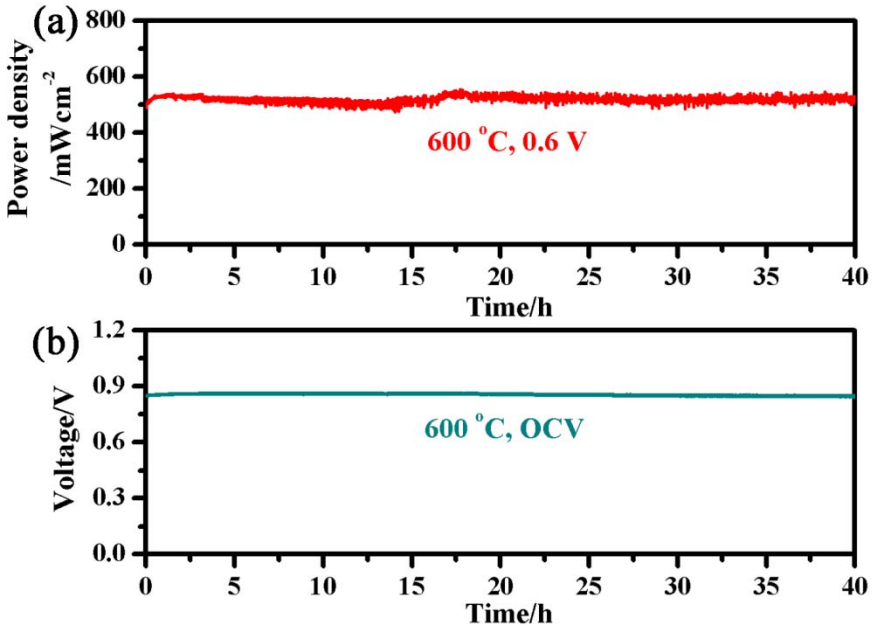

Table1

Electrolyte	Cathode	MPD/mWcm^{-2} (650 °C)	OCV/V (650 °C)	R_v/Ωcm^2 (650 °C)	R_p/Ωcm^2 (650 °C)	Ref.
BCY-GDC(molar ratio 1:1)	LSCF-BCY-GDC	240	0.82	—	—	30
SDC-BCY (90:10wt.%)	BCFN	159 (600°C)	0.9	—	—	31
BCY-SDC (25:75wt.%)	Ag	250 (550°C)	0.9	—	—	29
BCS-SDC (50:50wt.%)	SCT-SDC	475	0.88	—	—	23
BCI-GDC*(30:70wt.%)	SSC-SDC	260 (600 °C)	0.99(600 °C)	—	—	28
BCS-SDC (50:50wt.%)	SSC-SDC	345	0.971	0.446	0.212	19
BCS-SDC (20:80wt.%)	SSC-SDC	782	0.812	0.172	0.078	This work
BCS-SDC (35:65wt.%)	SSC-SDC	695	0.842	0.186	0.081	This work
BCS-SDC (50:50wt.%)	SSC-SDC	415	0.86	0.246	0.183	This work
BCS-SDC (65:35wt.%)	SSC-SDC	277	0.901	0.483	0.185	This work

$BaCo_{0.7}Fe_{0.2}Nb_{0.1}O_{3-\delta}$(BCFN), $BaCe_{0.8}Sm_{0.2}O_{3-\delta}$ (BCS), $Ce_{0.8}Gd_{0.2}O_{1.9}$(GDC), $Ce_{0.9}Gd_{0.1}O_{2-\delta}$ (GDC*), $SrCo_{0.9}Ti_{0.1}O_{3-\delta}$(SCT)

$La_{0.8}Sr_{0.4}Co_{0.2}Fe_{0.8}O_{3-\delta}$(LSCF), $Sm_{0.5}Sr_{0.5}CoO_{3-\delta}$ (SSC), $Ce_{0.8}Sm_{0.2}O_{1.9}$(SDC)